Proceedings of ASME Turbo Expo 2011
GT2011
June 6-10, 2011, Vancouver, British Columbia, Canada

GT2011-46230

EFFECT OF WAKE FLOW NON-UNIFORMITY ON WIND TURBINE PERFORMANCE AND AERODYNAMICS

S. Barber* **N. Chokani** **R.S. Abhari**

Laboratory for Energy Conversion,
Department of Mechanical and Process Engineering,
ETH Zurich,
Zurich.
Email: barbers@ethz.ch

ABSTRACT

Dynamically scaled experiments and numerical analyses are performed to study the effects of the wake from an upstream wind turbine on the aerodynamics and performance of a downstream wind turbine. The experiments are carried out in the dynamically-scaled wind turbine test facility at ETH Zurich. A 5-hole steady-state probe is used to characterize the cross-sectional distribution of velocity at different locations downstream of the wake-generating turbine. The performance of the downstream wind turbine is measured with an in-line torquemeter. The velocity field in the wind turbine wake is found to differ significantly from the velocity field assumed in numerical wake models. The velocity at hub-height does not increase monotonically up to the freestream velocity with downstream distance in the wake. Furthermore, the flowfield is found to vary significantly radially and azimuthally. The application of wake models that assume a constant axial velocity profile in the wake based on the measured hub-height velocity can lead to errors in Annual Energy Production predictions of the order of 5% for typical wind farms. The application of wake models that assume an axisymmetric Gaussian velocity profile could lead to prediction errors of the order of 20%. Thus modeling wind turbine wakes more accurately, in particular by accounting for radial variations correctly, could increase the accuracy of Annual Energy Production predictions by 5-20%.

NOMENCLATURE

A_{rotor}	Rotor area	[m^2]
$A_{channel}$	Channel cross-sectional area	[m^2]
C_P	Power coefficient	
D	Rotor diameter	[m]
Re	Reynolds number (3/4 chord)	
T_{rotor}	Rotor torque	[Nm]
V_0	Inflow velocity	[m/s]
V_x	Axial velocity	[m/s]
V_θ	Azimuthal velocity	[m/s]
V_r	Radial velocity	[m/s]
Ψ	Yaw angle	[°]
ϑ	Pitch angle	[°]
θ	Azimuth angle	[°]
ρ	Fluid density	[kg/m^3]
ω	Rotor rotational speed	[rad/s]
ω_z	Vorticity component in axial direction	[s^{-1}]

1. INTRODUCTION

Wind energy is the world's fastest growing source of electricity production; 160 GW of installed capacity was reached in 2009, an increase of 33% over 2008. In order for this growth to continue, wind energy projects must effectively take advantage of wind-rich sites. Limitations on available space mean that it is advantageous to develop wind farms with turbines spaced as closely as possible. However, a wind turbine produces a turbulent wake region downstream of its rotor, which can adversely affect the performance and lifetime of downstream wind turbines. Thus, a compromise to maximize the benefits due to economies of scale and minimize the losses due to wake interactions must be reached. This has led to international standards [1] that recommend an axial separation of adjacent wind turbines within a wind farm of 8-10 rotor diameters (8-10D). Power losses due to wake effects are expected to be of the order of 5-15% of the entire wind farm power generation [2].

* Corresponding author

Copyright © 2011 by ASME

Significant research has been undertaken in order to develop numerical models that predict wake effects for any given wind farm. Wind farm developers use these models in their initial site assessment to predict the Annual Energy Production (AEP). Accounting for wake effects increases the accuracy of AEP predictions and reduces investment risks and costs. Numerical wake models used in industry include the Jensen model [3], the Risoe engineering model [4], the Risoe WAsP model [5] and the ECN Wakefarm model [6,7]. For a more detailed description of these models, see [8]. One consideration in the development of the models is a compromise between computational load and accuracy of prediction such that the models are practical for industrial applications.

The models mentioned above are based on a two-dimensional inviscid analysis, where the wind turbine is modeled as a flat disc that reduces the velocity of the wind. The models focus on predicting the velocity deficit and wake expansion downstream of a wind turbine rotor, as these are considered to be the key factors related to wind farm performance. The wake is assumed to be circular and axi-symmetric and, except for the ECN model, the velocity profile is assumed to be constant in a radial direction. The predicted development of axial velocity in the wake, normalized with the freestream velocity, is shown in Fig. 1(a) for three models (Jensen, Frandsen and WAsP) at the same operating conditions. The curves differ slightly in shape, but all show a monotonic increase towards the freestream velocity. The ECN model predicts a Gaussian velocity profile at a downstream distance of 2.25D based on experimental data measured on a sub-scale model in a wind tunnel, as shown in Fig. 1(b) [6]. This profile then develops downstream of the rotor, with a distribution that is tuned to experimental measurements at hub-height in the same experiment, as shown in Fig. 1(c). These measurements were made on a 0.36 m diameter wind turbine in a wind tunnel. It can be seen that this model predicts a significantly larger velocity deficit than the other models, and that this is most pronounced from 2D to 4D downstream.

It is evident that predictions of velocity in the wake, whilst qualitatively similar, differ significantly quantitatively. This could lead to significantly different predictions of AEP for a given wind farm. A more detailed understanding of the wake's flowfield is required in order to improve these models and thereby to reduce wind farm investment risks and costs. This is achieved in the present work with a unique combination of experimental and numerical studies. This approach facilitates (a) making a direct link between the flowfield and the performance of a wind turbine placed in the wake to be made and (b) quantification of the impact of the assumptions made in wake models on the AEP prediction of a wind farm. This work is part of a broader effort at ETH Zurich that also involves field experiments and CFD modeling and which are reported elsewhere [9,10,11]. The experimental part of the present work was carried out using controlled measurements at the ETH Zurich dynamically-scaled wind turbine test facility. This is equipped with performance measurement and flowfield measurement capabilities as described in the next section. The numerical work was carried out using the in-house ETH Zurich unsteady Blade Element Momentum (BEM) tool, which allows the input of any three-dimensional flowfields at the rotor inlet plane.

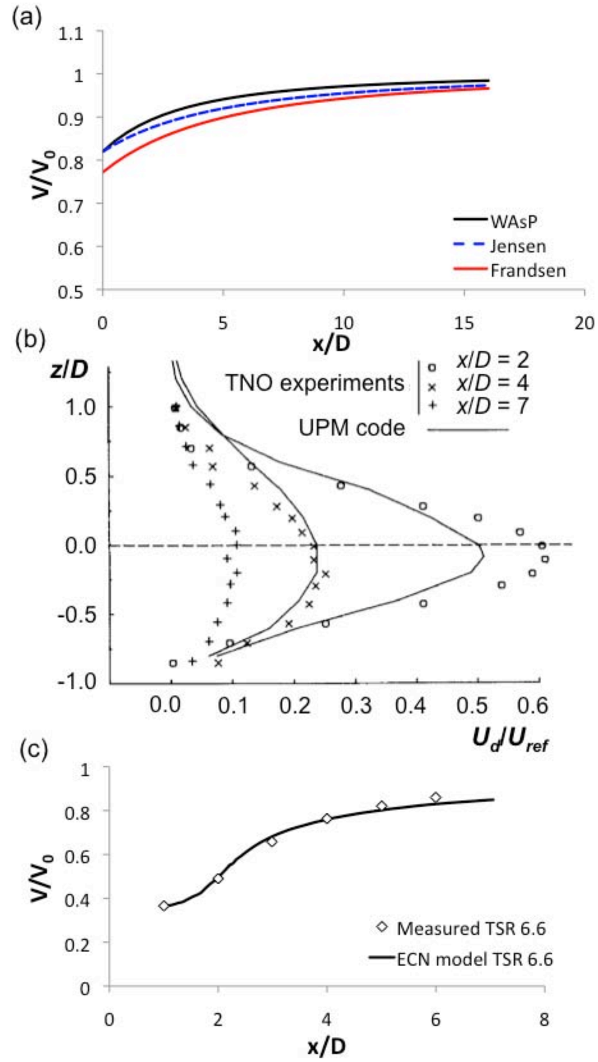

Fig. 1 (a) Normalized axial velocity in the wake for Jensen, Frandsen and WAsP models; **(b)** ECN model velocity profile compared to measurements; **(c)** ECN model showing development of velocity in the wake compared to measurements [6].

2. SET-UP

2.1. The ETH Zurich Dynamically-Scaled Wind Turbine Test Facility

The experimental part of this work was carried out in the dynamically-scaled wind turbine test facility at the Laboratory for Energy Conversion (LEC) of ETH Zurich (Fig. 2(a)). The facility is described in a previous paper [12], but its salient features are detailed here for completeness.

Copyright © 2011 by ASME

Tandem turbine arrangement

In this work, the facility was operated with two wind turbine models in a tandem arrangement as shown in Fig. 2(b). The convention for axial separation between the two wind turbines (x) is marked on the figure. In the facility, the two 0.3 m diameter wind turbine models can be mounted either separately or in a tandem arrangement on a carriage that moves above a 40 m long, 1 m wide and 1 m deep channel of water. The velocity of the carriage can be specified to up to 3 m/s (± 1%). The water temperature was 19 ^oC ± 0.5 ^oC throughout the measurement campaign. The turbulence intensity of the flow was zero. Both rotors were placed in the center of the channel and the blockage ratio ($A_{rotor}/A_{channel}$) of each rotor was 7.1%, which is less than the upper limit of 7.5% required for blockage corrections [13]. The Froude number of the channel ranges from 0.03 up to 0.92 for the maximum velocity of 3 m/s; thus surface and blockage effects are negligible [12].

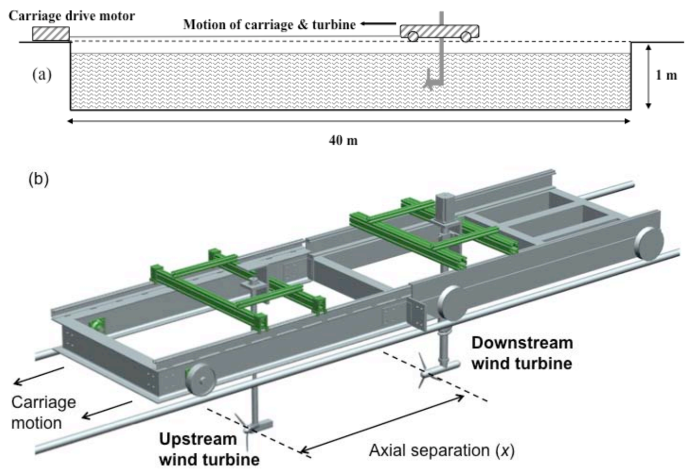

Fig. 2. ETH Zurich dynamically-scaled wind turbine test facility: (a) Schematic diagram; (b) Tandem turbine arrangement.

The blade geometry of the three-bladed wind turbines matches the National Renewable Energy Laboratories (NREL) Phase VI rotor from 25% to 100% span [14]. From the hub to 25% span the blade profile was modified in order to improve the structural rigidity. The blades of both wind turbines are interchangeable and the pitch angle can be set with an accuracy of $\pm 1^o$. For the current tests the blade pitch of both turbines was set to 0^o following systematic tests to find the pitch giving the optimal power coefficient curve. The rotational speeds of both wind turbines are controlled by DC motors. The desired tip speed ratio of the wind turbine can thus be accurately specified. In this study, the maximum turbine rotational speed was 800 rpm (± 3 rpm), which avoided cavitation.

The hub and nacelle geometry of the upstream turbine match that of the NREL Experiment [14]. The hub of the downstream turbine was increased slightly from 14% to 18% of the rotor radius to allow measurement of the torque as described below.

The Reynolds number based on mean chord at the optimal tip speed ratio of 6.0 is 1.5×10^5 for both turbines. As a comparison, the same size model in a wind tunnel with the same freestream flow conditions would have a Reynolds number of 10,000. Many full-scale wind turbines reach a Reynolds number of the order of 5.0×10^6. It is evident that the full-scale non-dimensional parameters are more closely reached in the ETH Zurich facility than in a wind tunnel.

Performance measurements

In this work, the performance of the downstream wind turbine was measured in the wake of the upstream wind turbine. This was done using an in-line, contactless miniature torquemeter installed on the shaft, as described in more detail in [12]. The measurement range is 0-5 Nm (accuracy ± 0.1%). The power coefficient (C_P) is determined as follows:

$$C_P = \frac{T_{rotor}\omega}{\frac{1}{2}\rho V_0^3 A_{rotor}} \tag{1}$$

where T_{rotor} is the rotor torque (Nm), ω the rotor rotational speed (rad/s), A_{rotor} the cross-sectional area of the rotor (m^2), V_0 the inflow velocity (m/s) and ρ the fluid density (kg/m^3). The relative errors of the C_P and tip speed ratio measurements arise from the errors in the translational velocity (±1%), rotational velocity (±0.4%), torque (±0.1%) and water temperature (±0.2%). The worst-case relative errors were found to be 0.4% in power, 3.0% in C_P and 1.1% in tip speed ratio.

The C_P vs. tip speed ratio curve for the downstream wind turbine in freestream flow is shown in Fig. 3. Typical behavior for a wind turbine with a peak in power coefficient of 0.42 is seen at a tip speed ratio of 6.28.

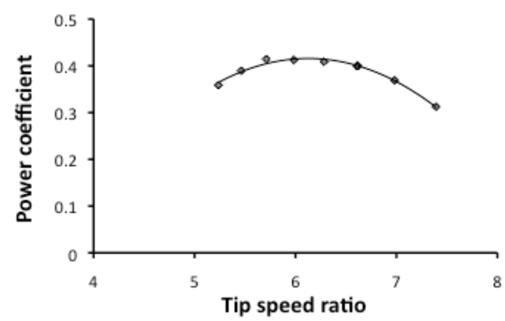

Fig. 3. C_P vs. tip speed ratio curve for the downstream wind turbine in freestream conditions.

Flowfield measurements

Flowfield measurements in the wake of the upstream wind turbine without the downstream wind turbine were made with a 5-hole steady-state pressure probe (5H-SSP). The probe has a head diameter of 5.5 mm and geometry as shown in Fig. 4(a).

 Copyright © 2011 by ASME

The conventions for the flow angles, pitch (ϑ) and yaw (Ψ), are also shown on the figure. The aerodynamic calibration of the probe was carried out in the fully automated free-jet calibration facility at the Laboratory for Energy Conversion, ETH Zurich (see [15] for a full description of the facility). In this facility, the probe is installed on a three-axis traversing system (lateral motion, yaw angle and pitch angle motion) in order to rotate the probe relative to the fixed jet. The automatic calibration procedure follows a pre-defined measurement grid for different probe yaw and pitch angles. For this probe, the set of calibration data was taken on a homogenous grid that covered ±20° in yaw and pitch angles, for a Mach number of 0.13, matching the Reynolds number in the wind turbine test facility. Local static pressure, total pressure and pitch and yaw angles are derived from coefficients that are calculated directly from local pressure measurements at the five holes of the probe. These coefficients are then used to calculate the static pressure, total pressure and pitch and yaw angles for each measurement made in the wind turbine test facility. The total velocity can then be computed from the static and total pressure values [16]. The calibration curves of the 5H-SSP are shown in Fig. 4(b).

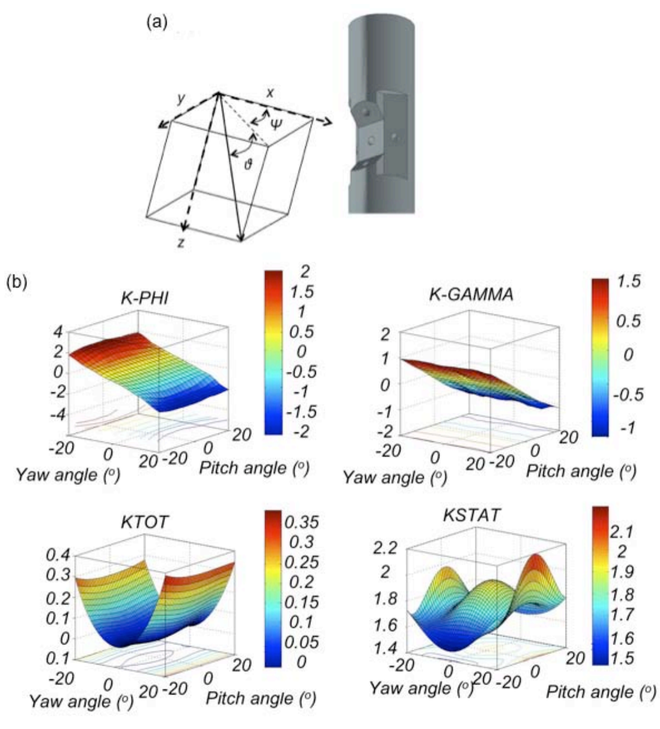

Fig. 4. (a) Head geometry of 5H-SSP; **(b)** Aero calibration coefficients.

The five flowfield pressures are independently measured using five Keller Series 35X relative pressure transducers, referenced to an absolute pressure transducer. Purging of air was carried out before each measurement campaign and the signals were monitored in real time to avoid measurement errors due to leakage. Each measurement was made over a period of 5 seconds.

A series of measurements in the freestream (without the wind turbines) over 72 points in a measurement plane the size of half the rotor (semi-circular radius 0.15 m) verified that the inflow velocity matched the desired carriage velocity within ±4%. The pitch and yaw angles remained in the range ±1°. Preceding each measurement campaign, the freestream velocity in the center of the channel was measured three times, and all subsequent measurements were referenced to the average of these measurements. This resulted in flowfield measurements that were repeatable to ±1%.

In this work, flowfield measurements were made with the 5H-SSP at 109 points according to the cylindrical grid shown in Fig. 5 (view from behind) in two planes at 2D and 11D downstream of the upstream wind turbine (without the presence of the downstream wind turbine). The lines making up the grid have an azimuthal separation of 30° and variable radial spacing. The rotor and hub positions are marked as circles on the figure and the tower position is marked as a rectangle.

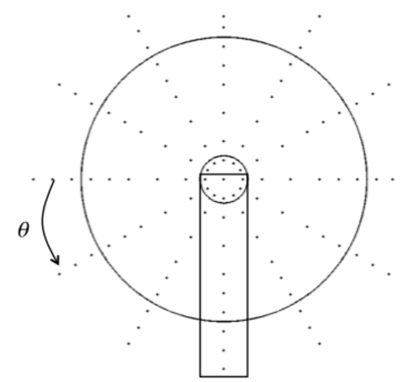

Fig. 5. Grid for plane measurements.

2.2. ETH Zurich Unsteady BEM Code

The numerical part of this work was carried out with the in-house unsteady Blade Element Method (BEM) code of ETH Zurich [17]. BEM theory involves analysis of a rotor in annular segments, followed by a summation of the resulting forces over all of the segments to find the total forces acting on the rotor. It is based on the assumption that the flow at a given annulus does not affect the flow at adjacent annuli. A flow-chart for this process is shown in Fig. 6.

The BEM code includes Prandtl's tip loss factor and Glauert's correction for high axial induction factors [18]. A three-dimensional velocity field can be specified at the inflow plane. This velocity field is then linearly interpolated for each given blade section and azimuth position. The BEM code has been validated by comparison with NREL's PROPID code [14] using two-dimensional airfoil data for the S809 airfoil at $Re = 1 \times 10^6$ [19] as shown in Fig. 7. This airfoil configuration is representative of the NREL experimental set-up [14]. The differences between the BEM and PROPID codes at low tip speed ratio (< 4.5) are due to a lack of airfoil data at high angles

 Copyright © 2011 by ASME

of attack. For the remainder of the work, airfoil data was taken for the S809 profile at Re = 300,000 to match the experimental conditions as closely as possible [20] and the rotor dimensions were specified to match the experimental set-up.

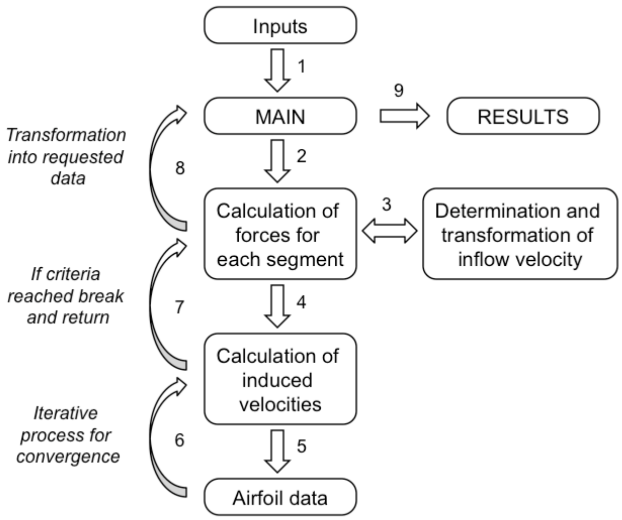

Fig. 6. Flow-chart of the unsteady BEM method.

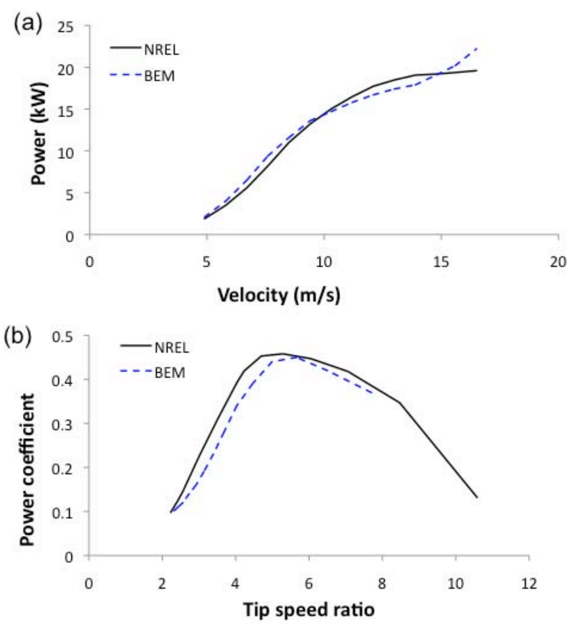

Fig. 7. Unsteady BEM code predictions compared to NREL PROPID for (a) Power vs. velocity; **(b)** Power coefficient vs. tip speed ratio.

3. RESULTS AND DISCUSSION

3.1. Wind Turbine Performance

In order to represent wind farm conditions in the ETH Zurich dynamically-scaled wind turbine test facility, the performance of a wind turbine in the wake of an upstream wind turbine was examined at a range of axial separations. For fixed-speed operation, the presence of the upstream wind turbine is seen to have a significant effect on the performance of the downstream turbine, as shown in Fig. 8. The power of the downstream wind turbine is in the range of 20-40% of the freestream power up to a separation of 9D. For larger axial separations, the power starts to rapidly increase towards 100% of freestream. Thus, even if a downstream wind turbine were placed at an axial separation distance of 10D, as recommended in [1], power losses of the order of 50-60% of the freestream power would be expected for wind farms sited in locations with very low turbulence intensity.

In order to examine variable-speed operation, both wind turbines were set to operate at rotational speeds corresponding to their optimal tip speed ratio. The optimal rotational speed for the downstream wind turbine was calculated from the measured velocity at hub-height as seen by the downstream wind turbine (without the presence of the downstream wind turbine). This corresponds to the operational mode of most variable speed turbines. The measured evolution of normalized hub-height axial velocity in the wind turbine wake is shown in Fig. 9, compared to two of the wake models discussed in the introduction. The wake models all under-predict the velocity deficit at hub-height compared to the experiments. The measured velocity decreases up to 7D downstream; further downstream the velocity increases rapidly towards the freestream value. At 7D downstream, the shear mixing layer has reached the center line and transfers higher velocity flow towards the center. This mixing process should be considered in order to improve the accuracy of numerical wake models. The reader is referred to a previous paper by the author [21] for more details.

For variable-speed operation, the normalized power of the downstream turbine is shown in Fig. 8 compared to the results for a fixed-speed turbine. Operating at variable speed can result in up to a 15% increase in freestream power compared to operating at fixed speed. This is due to the increased power coefficient caused by optimizing the tip speed ratio. However, this increase reduces to almost zero as the axial separation increases from 7D to 11D. This is due to the fairly flat shape of the C_P vs. tip speed ratio curve for this wind turbine: as the axial separation increases from 7D to 11D, the inflow velocity increases and the tip speed ratio decreases correspondingly. As the inflow velocity is smaller than the design inflow velocity, the downstream wind turbine is operating on the right-hand side of the power coefficient curve, at tip speed ratios larger than the optimal value. Thus increasing the axial separation from 7D to 11D involves climbing up the right-hand side of the curve in Fig. 3 from right to left. The curve flattens out close to the optimal point, and therefore the losses between fixed- and variable-speed operation approach zero.

Even though a power increase can be achieved by operating at variable speed, losses of up to 60% of freestream power are nevertheless observed. This reduction corresponds well with power measurements on turbines within the Danish Horns Rev wind farm [22]. For higher freestream turbulence levels, this reduction in power is expected to be smaller, due to

 Copyright © 2011 by ASME

accelerated mixing in the wake. This should, however, be investigated in more detail. The aerodynamics relating to these losses are investigated further in the subsequent sections of this paper.

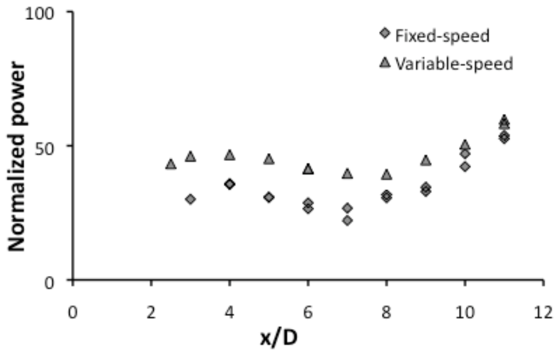

Fig. 8. Normalized power vs. axial downstream distance in the wake of the upstream wind turbine for fixed-speed compared to variable-speed downstream wind turbines.

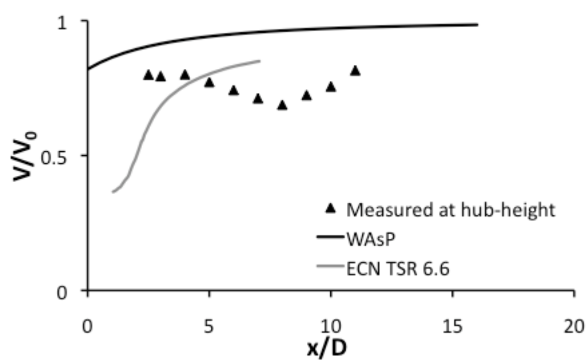

Fig. 9. Normalized velocity vs. axial downstream distance in the wake of the upstream wind turbine.

3.2. Examination of Aerodynamics

Figure 10(a) shows the measured axial velocity in the plane 2D downstream of the upstream turbine. The observer's view is upstream (so that the rotor rotates in a clockwise direction) and velocity is normalized with the freestream velocity. The flowfield is clearly radially and azimuthally non-uniform. Figure 10(b) shows the variation in velocity with the radial position at $\theta = 0^o$, 30^o and 90^o. It can be seen that the minimum axial velocity is located at approximately 40-60% span. This offset occurs as the flow accelerates around the slower wake of the nacelle. Comparison of these three velocity profiles also highlights the asymmetry of the flow due to the tower in the bottom half of the rotor, especially in the tip region from 80% span outwards. This region is not symmetric about the tower, but is skewed by approximately 10^o in the direction of rotor rotation. The low-pressure wake region behind the tower draws the flow inwards and results in a speed-up around the tower wake periphery. The speed-up region outside the wake is also seen in Fig. 10(b), and the speed-up reaches a magnitude of up to 5% of the freestream velocity. The Gaussian profile predicted by the ECN model [7], given the performance characteristics and dimensions of the present wind turbine, is also shown in Fig. 10(b). Although the predicted hub-height velocity matches well with the measurements, the predicted velocities over the mid-span range ($0.3 < r/R < 0.8$) are clearly very different. The impact of this assumed Gaussian profile is assessed in a subsequent section of this work.

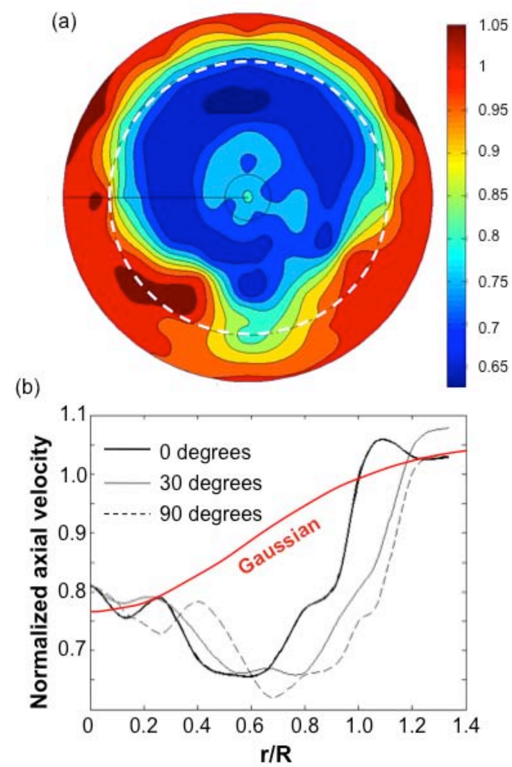

Fig. 10. (a) Normalized axial velocity for a plane 2D downstream; **(b)** Variation with radial position at 0^o, 30^o and 90^o.

Fig. 11(a) shows the normalized axial velocity in the plane 11D downstream of the upstream turbine. It is clear that the flow has mixed out more compared to the more upstream measurement at 2D (Fig. 10); however, there is still a significant influence of the rotor on the flow. The flowfield is still radially and azimuthally non-uniform. The region of slow-moving flow in the wake has mixed out, elongated and become skewed by an angle of approximately 30^o in a direction opposite to the rotor rotation. In Fig. 11(b), the variation in velocity with the radial position is shown at $\theta = 0^o$, 30^o and 90^o. The large fluctuations present in the profiles highlight the loss of flow structure due to mixing.

Copyright © 2011 by ASME

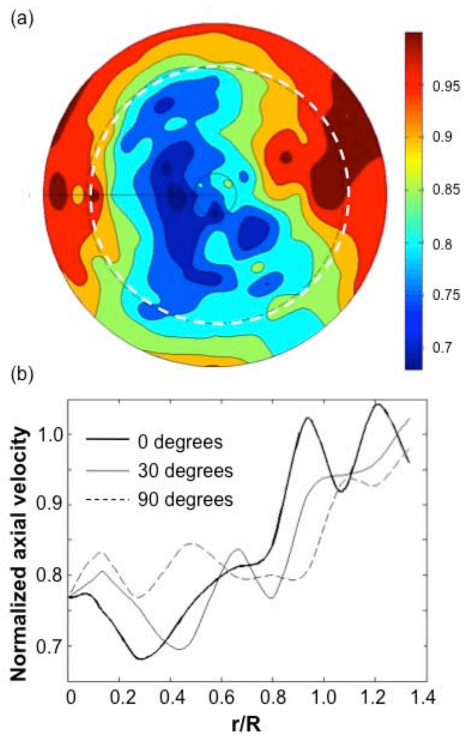

Fig. 11. (a) Normalized axial velocity for a plane 11D downstream; **(b)** Variation with radial position at 0°, 30° and 90°.

The pitch and yaw angles range between –6° & 8°, and between -7° & 4°, respectively, for 2D. For 11D, the pitch and yaw angles range between –2° & 3°, and between -5° & 5°, respectively. The normalized radial and azimuthal velocities derived from these flow angles for 2D and 11D are shown in Fig. 12(a) and 12(b). A positive radial velocity refers to flow moving outwards from the rotor center, whereas a positive azimuthal velocity refers to an anticlockwise motion; that is, in the opposite direction to the rotor rotation.

These velocity components have a maximum magnitude of one-tenth of the total velocity. For 2D, distinct flow structures can be seen; the flow is being entrained towards the center between $\theta = 0^o$ and 90^o and between $\theta = 180^o$ and 270^o. In the other sections of the plane, the flow is being driven outwards. This flow structure suggests vortical behavior, which will be further examined. For 11D, these distinct structures have mixed out, and the magnitude of the radial and azimuthal velocity has reduced to approximately half the magnitude of the 2D case.

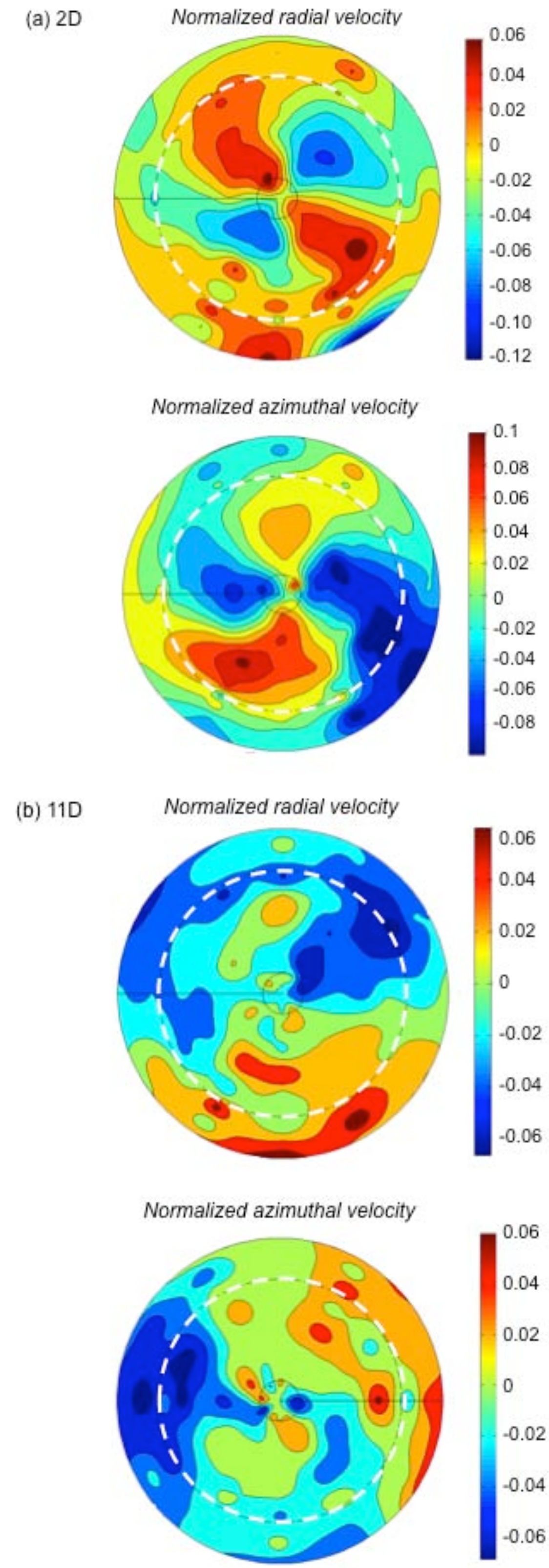

Fig. 12. Normalized radial and azimuthal velocity components at **(a)** 2D and **(b)** 11D downstream in the wake.

Copyright © 2011 by ASME

The flow structures described above are examined in more detail in Fig. 13, which shows the velocity vectors based on the radial and azimuthal velocity components at the measurement planes x = 2D and 11D. The maximum vector length has a magnitude of 15% of the freestream velocity. Coherent flow structures can be clearly seen. At 2D, two regions of counter-rotating fluid can be observed; one region moving downwards in the area of the tower and one moving upwards and to the left. By 11D, these regions are weaker and have rotated approximately 30^o in the opposite direction to the rotor rotation. This is indicative of low frequency meandering of the wake, and should be further investigated.

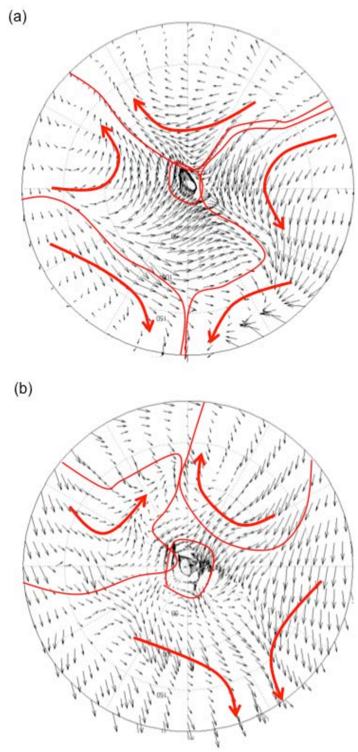

Fig. 13. Radial and azimuthal velocity components at **(a)** 2D and **(b)** 11D downstream in the wake.

The structures in the wake at 2D and 11D are further investigated by calculating the component of vorticity in the axial direction (ω_z):

$$\omega_z = \frac{1}{r}\frac{\partial(rV_\theta)}{\partial r} - \frac{1}{r}\frac{\partial V_r}{\partial \theta} \tag{2}$$

where V_θ = azimuthal velocity (m/s) and V_r = radial velocity (m/s). Figure 14 shows that there are two regions where counter-rotating vortices occur in the 2D plane. The first region is downstream of the nacelle, where a counter-rotating vortex is formed downstream of the square-ended nacelle. The second region is downstream of the tower, where a horseshoe vortex can be seen at either side of the tower. Such a horseshoe vortex is expected to be formed downstream of a truncated cylinder, as shown in the time-averaged schematic diagram in Fig. 15 [23]. In the measurements undertaken in this paper, the cylindrical wind turbine tower is truncated by an airfoil-shaped profile attached to the tower. This prevents vortex shedding and other water surface effects in the experimental facility, which would not be present in reality. At 11D, this horseshoe vortex has disappeared, but the counter-rotating vortices in the center due to the nacelle remain (but with reduced magnitude). The presence of these vortical structures implies that are losses that may have an impact on the performance of a downstream wind turbine.

The impact of these measured flowfields on the performance of a downstream wind turbine is examined in the next section.

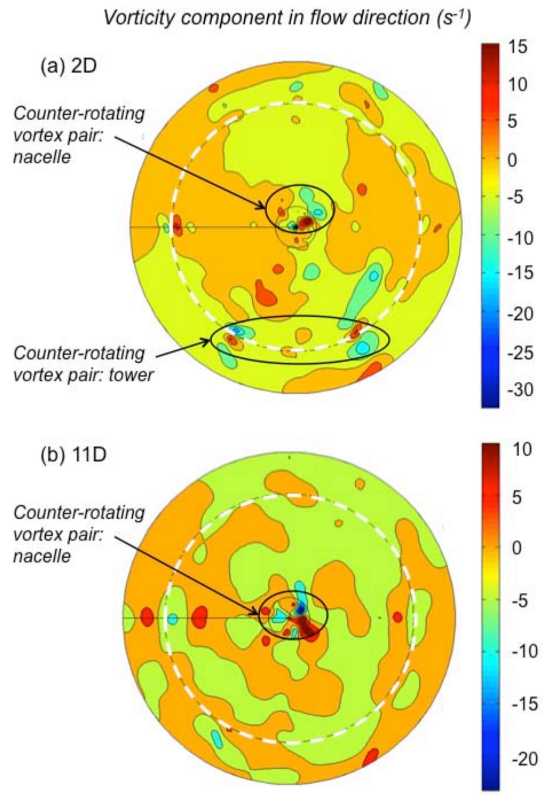

Fig. 14. Vorticity components in the axial direction at **(a)** 2D and **(b)** 11D downstream in the wake.

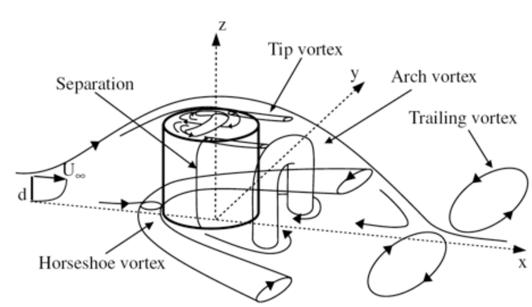

Fig. 15. Schematic diagram of time-averaged flow over truncated cylinder [23].

Copyright © 2011 by ASME

3.3. Impact of Flow Non-Uniformity on Performance

An examination of the aerodynamics in the previous section has shown that the flowfield in a wind turbine wake is different from the flowfield assumed in wake models. The main features observed in the measured flowfield that are absent in assumed flowfields of wake models are summarized as follows:

A. The wake velocity field contains in-plane components and coherent vortical structures that may not be negligible;
B. The measured wake velocity profile is not constant;
C. The measured wake velocity profile is not Gaussian;
D. The wake velocity field is not axisymmetric.

In this section, the BEM code is applied in order to examine the impact of these differences on the predicted wind turbine performance. This allows for quantification of potential improvements that could be made to wake models by basing the velocity profiles on more detailed experimental measurements such as the ones made in the present work. For each prediction, the rotational velocity of the wind turbine was set to give the optimal tip speed ratio based on the hub-height velocity.

The power production is first predicted using the measured axial velocity flowfields as inputs to the BEM code. The predicted power is compared with the measured power in Table 1. The predicted and measured values differ by 1-2%. These differences are within the repeatability of the flowfield measurements. In Fig. 16, the predicted variation of the incidence across the span is shown. The incidence is averaged over one revolution. The reduction in incidence by up to 2^o from 20% to 80% span from 11D to 2D explains the lower power production at 2D.

Table 1. Predicted power compared to measured power.

	Power relative to freestream power		
x/D	Measured	Predicted	% Difference
2	43	45	2
11	59	58	1

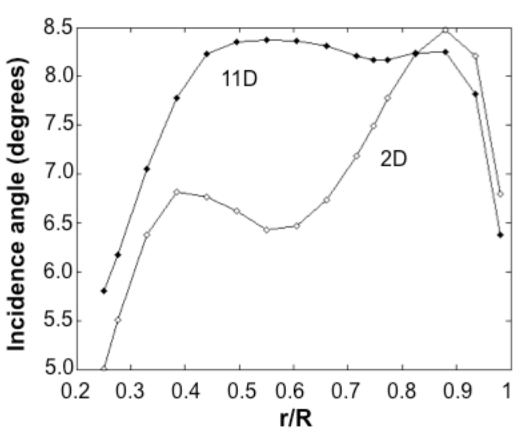

Fig. 16. Average incidence over rotor for one revolution: 2D compared to 11D.

The impact of assumptions A to D on the power prediction was calculated in each case by entering a new velocity field into the BEM code corresponding to each assumption. The resulting power production was then compared with the power production predicted for the measured flowfield.

The impact of assumption A on the predicted wind turbine performance was tested by predicting the power with the radial and azimuthal velocity components included. This assumption was found to have a negligible impact on the power production (±0.5%). The impact of assumption B on the predicted wind turbine performance was tested by creating a flowfield of constant velocity equal to that measured at hub-height. This assumption was found to over-estimate the power by 7% for 2D and 3% for 11D. The impact of assumption C on the predicted wind turbine performance was tested by creating an axisymmetric Gaussian distribution flowfield as specified in the ECN model for 2D only, as this flowfield is only defined for 2.25D [7]. This assumption was found to over-predict the power by 30%. The impact of assumption D on the predicted wind turbine performance was tested by creating axisymmetric flowfields by averaging the measured data at each radial location azimuthally over a full rotation. This assumption was found to over-predict the power by 0.3% for 2D and under-predict the power by 0.5% for 11D. Thus, the assumption of axisymmetry itself has a negligible impact on performance prediction.

The percentage differences between the predicted power for each assumption and the predicted power for the measured axial velocity field are summarized in Table 2 for 2D and 11D.

Table 2. Percentage variation from measurements for assumptions A to D.

Case	% variation from measurements	
	2D	11D
A	+0.5	-0.5
B	+7	+3
C	+30	N/A
D	+0.3	+0.5

These results are converted into uncertainties for the prediction of AEP for a typical wind farm of 8 columns by 10 rows of wind turbines (matching the layout of the Danish offshore wind farm, Horns Rev [22]) in Fig. 17. This assumes no additional effects from the further overlapping of two or more wakes. The uncertainty for AEP prediction is lower than that of the power prediction of a single wind turbine due to the fact that the wind farm has 8 of its 80 wind turbines exposed to the freestream and which are not affected by upstream wakes. Note that the "constant inflow" and "axisymmetric" assumptions apply for axial separations between 2D and 11D, whereas the "Gaussian" assumption only applies for an axial separation of 2D.

It is clear that the assumptions made in many commonly-used wake models could have a significant negative impact on the accuracy of AEP predictions for a wind farm and thus on project costs and risks. It is thus important to model these

 Copyright © 2011 by ASME

flowfields more accurately. This is the subject of ongoing work at the ETH Zurich dynamically-scaled wind turbine test facility.

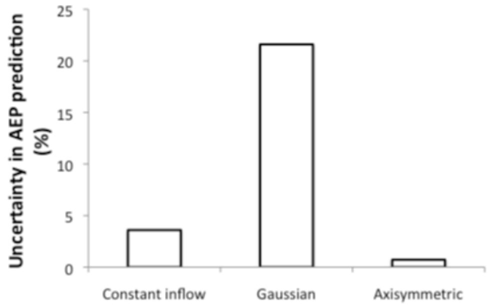

Fig. 17. Summary of errors in magnitudes of power and Annual Energy Productions predictions due to common wake model assumptions.

4. CONCLUSIONS

- The velocity field in wind turbine wakes differs significantly from the velocity field assumed in numerical wake models. The main differences between the measured and modeled velocity fields are that (a) the velocity at hub-height does not increase monotonically up to the freestream velocity with downstream distance in the wake and (b) the flowfield varies radially and azimuthally.

- The application of wake models that assume a constant axial velocity profile in the wake based on the measured hub-height velocity can lead to errors in Annual Energy Production predictions of the order of 5% for typical wind farms. The application of wake models that assume an axisymmetric Gaussian velocity profile could lead to prediction errors of the order of 20%. Thus modeling wind turbine wakes more accurately, in particular by accounting for radial variations correctly, could increase the accuracy of Annual Energy Production predictions by 5-20%.

ACKNOWLEDGMENTS

The authors would like to thank the Swiss Federal Office of Energy for supporting this project (BFE-102744). The support of Michel Mansour (LEC) and of Mohamed Farhat and Henri-Pascal Mombelli (EPFL) are greatly appreciated, as are the technical contributions of Flori Alickaj, Evgeni Kochman, Christian Kress, Thomas Kunzle, Cornel Reshef and Claudio Troller.

REFERENCES

[1] IEC Wind Turbine Generator Systems, Part 1: Wind Turbine Safety and Design, 1998, *IEC International Standard 61400-11*.

[2] Barthelmie, R., Larsen, G., Pryor, S., Jørgensen, H., Bergström, H., Schlez, W., Rados, K., Lange, B., Vølund, P., Necelmann, S., Mogensen, S., Schepers, G., Hegberg, T., Folkerts, L. and Magnusson, M., 2004, "ENDOW (Efficient Development of Offshore Wind Farms); Modelling Wake and Boundary Layer Interactions", *Wind Energy*, Vol. **7**, pp. 225-245.

[3] Jensen, N.O., 1983, "A Note on Wind Turbine Interaction", *Risø-M-2411*, Risoø National Laboratory, Roskilde, Denmark.

[4] Frandsen, S., Barthelmie, R., Pryor, S., Rathmann, O., Larsen, S., Højstrup, J. and Thøgersen, M., 2004, "Analytical Modeling of Wind Speed Deficit in Large Offshore Wind Farms", *Scientific Proceedings of the European Wind Energy Conference and Exhibition*, London, United Kingdom, pp. 6-11.

[5] Larsen, G.C., Madsen, H.A. and Sørensen, N.N., 2003, "Mean Wake Deficit in the Near Field, *Proceedings of the European Wind Energy Conference*, Madrid, Spain, European Wind Energy Association, CD-ROM.

[6] Schepers, J.G., 2003, "ENDOW: Validation and Improvement of ECN's Wake Model", *ECN-C-03-034*.

[7] Crespo, A., Hernandez, J., Fraga, E. and Andreu, C., 1988, "Experimental Validation of the UPM Computer Code to Calculate Wind Turbine Wakes and Comparison with Other Models", *Journal of Wind Engineering and Industrial Aerodynamics*, Vol. **27**, pp. 77-88.

[8] Barthelmie, R.J., Folkerts, L., Larsen, G.C., Rados, K., Pryor, S.C., Frandsen, S.T., Lange, B. and Schepers, G., 2006, "Comparison of Wake Model Simulations with Offshore Wind Turbine Wake Profiles Measured by SODAR", *Journal of Atmospheric and Oceanic Technology*, Vol. **23**, pp. 888-901.

[9] Kocer, G., Mansour, M., Chokani, N., Abhari, R.S. and Müller, M., 2011 "Full-Scale Wind Turbine Wake Measurements Using an Instrumented UAV", to appear at the European Wind Energy Association, March 2011.

[10] Mansour, M., Kocer, G., Lenherr, C., Chokani, N. and Abhari, R.S., 2011, "Seven-Sensor Fast-Response Probe for Full-Scale Wind Turbine Flowfield Measurements", ASME Journal for Gas Turbines and Power, Vol. 133.

[11] Jafari, S., Chokani, N. and Abhari, R.S., 2010 "Terrain Effect on Wind Flow: Simulations with an Immersed Boundary Method", submitted IGTI paper number GT2011-46240.

[12] Barber, S., Wang, Y., Jafari, S., Chokani, N. and Abhari, R.S., 2011, "The Impact of Ice Formation on Wind Turbine Performance and Aerodynamics", *Journal of Solar Energy* 133(1).

[13] Rae, W.H., Pope, A. and Barlow, J.B., 1999, *Low-Speed Wind Tunnel Testing*, John Wiley & Sons, New York, USA, Chap. 10.

[14] Giguere, P., and Selig, M.S., 1999, "Design of a Tapered and Twisted Blade for the NREL Combined Experiment Rotor," *NREL Technical Report No. SR-500-26173*.

[15] Kupferschmied, P., Köppel, P., Roduner, C. and Gyarmathy, G., 2000, "On the Development and Application of the Fast-Response Aerodynamic Probe System in Turbomachines – Part 1: The Measurement System", *Journal of Turbomachinery*, Vol. **122**, pp. 505-516.

 Copyright © 2011 by ASME

[16] Treiber, M., Kupferschmied, P. and Gyarmathy, G., 1998, "Analysis of Error Propagation Arising from Measurements with a Miniature Pneumatic 5-Hole Probe", *Proceedings of the 14th Symposium on Measuring Techniques for Transonic and Supersonic Flows in Cascades and Turbomachines*, Limerick, Ireland.

[17] Kochman, E., 2010, "Effect of Shear Profile and Yaw Angle on Wind Turbine Performance", LEC internal report, ETH Zurich, Switzerland.

[18] Burton, T., Sharpe, D., Jenkins, N. and Bossanyi, E., 2001, *Handbook of Wind Energy*, John Wiley & Sons, New York, USA.

[19] Somers, D.M., 1997, "Design and Experimental Results for the S809 Airfoil", *NREL technical report NREL/SR-440-6918*.

[20] Butterfield, C.P., Musial W.P. and Simms, D.A., 1992, "Combined Experiment Phase I Final Report", *NREL technical report NREUTP-257-4655*.

[21] Barber, S., Chokani, N. and Abhari, R.S., 2011, "Wind Turbine Performance & Aerodynamics in Wakes Within Wind Farms", *Scientific Proceedings of the European Wind Energy Conference*, CD-ROM.

[22] Barthelmie, R.J., Hansen, K., Frandsen, S.T., Rathmann, O., Schepers, J.G., Schlez, W., Phillips, J., Rado, K., Zervos, A., Politis, E.S. and Chaviaropoulos, P.K., 2009, "Modelling and Measuring Flow and Wind Turbine Wakes in Large Wind Farms Offshore", *Wind Energy*, Vol. **12**, pp. 431-444.

[23] Pattenden, R.J., Turnock, S.R. and Zhang, X., 2005, "Measurements of the Flow Over a Low-Aspect-Ratio Cylinder Mounted on a Ground Plane", *Experiments in Fluids*, Vol. **39**, pp. 10–21.

Copyright © 2011 by ASME